Time-dependent mean-field description for multiple charge-transfer processes in Ar^{8+}-Ar collisions

R. Nagano,[1] K. Yabana,[2] T. Tazawa,[3] and Y. Abe[4]
[1]*Graduate School of Science and Technology, Niigata University, Niigata 950-2181, Japan*
[2]*Institute of Physics, University of Tsukuba, Tsukuba 305-8571, Japan*
[3]*Department of Physics, Yamaguchi University, Yamaguchi 753-8511, Japan*
[4]*Yukawa Institute for Theoretical Physics, Kyoto University, Kyoto 606-8502, Japan*
(Received 4 August 2000; published 15 November 2000)

We present a quantum-mechanical study of multiple-electron transfer processes in collisions between a highly charged ion and an atom, taking Ar^{8+}-Ar collisions as an example. We employ time-dependent mean-field theories for this purpose, with different levels of approximation for the exchange effect. The time-dependent single-electron equation is solved directly by a discretization of the three-dimensional Cartesian coordinate into a uniform mesh. Calculations for various physical situations specified by the incident energy and the impact parameter are presented to elucidate the reaction mechanisms. They provide us with intuitive pictures of the electronic dynamics as well as a microscopic understanding of the reaction mechanisms. We also compare results with different treatments of the exchange effect to learn the sensitivity of our results on the possible uncertainty of the theories.

PACS number(s): 34.70.+e, 34.10.+x, 31.15.Fx

I. INTRODUCTION

Multiple charge-transfer processes which take place in the collisions of highly charged ions provide an interesting opportunity to investigate the time-dependent many-electron dynamics. Basic features of the charge-transfer processes have been well described by the molecular classical overbarrier model [1] in which the electron motion is assumed to be governed by a one-body field for electrons. The potential barrier height as well as the ionization potential are the basic elements in the model.

Theoretically, a fully quantum-mechanical close-coupling calculation has been rapidly developing. Analyses, however, were limited to one- and two-electron-transfer processes. Apparently, approximate theories are required to describe the dynamics of multiple electron-transfer processes. Several frameworks based on the time-dependent mean-field picture have been applied so far. For example, the time-dependent Hartree-Fock (TDHF) theory has been applied to the dynamics of two-electron systems [2].

We recently reported on a calculation of the multiple charge-transfer process in the time-dependent local-density approximation, taking $Ar^{8+}+Ar$ collisions as an example [3]. In that report, we focused upon showing the feasibility of the calculation as well as a reasonable reproduction of the measurements. The purpose of the present paper is to provide a detailed explanation of the method and to investigate the electronic dynamics for various physical conditions. In particular, we will compare results with different levels of approximation for the nonlocal exchange effect, and discuss their significance on observables of the charge-transfer reaction.

The time-dependent local-density approximation (TDLDA) is considered as an extension of static density-functional theory, so as to treat the time-dependent dynamics of many-electron systems [4]. The calculation employing the same exchange and correlation potential as that for the static problem is known as the adiabatic local-density approximation, and has been successful in describing the optical responses of various systems including atoms [5], molecules, atomic clusters [6], and dielectric functions [7]. Recently, it was also applied to the dynamics beyond the perturbative treatment such as the ionization of atoms and clusters by a short pulse laser [8] and by a highly charged ion [9].

In the simplest local-density approximation (LDA), the self-consistent potential falls off exponentially at large distance, and does not show the correct asymptotic behavior. Also the highest occupied orbital energy of the static Kohn-Sham orbital does not coincide with the ionization potential. Since the asymptotic Coulomb potential and the ionization potential are the basic elements of the classical overbarrier model, treatments beyond the simple LDA are highly desired to clarify the reliability of the calculated results. Indeed, the sensitivity of the results on the treatment of the exchange was stressed recently for one- and two-electron-transfer processes [10].

In this paper, we report two calculations with an improved treatment of exchange beyond the simple LDA. One is an approach based on the self-interaction correction combined with an approximate construction of the optimized effective potential [11]. The other is an exact treatment of the nonlocal exchange potential in the time-dependent Hartree-Fock theory. We will discuss the accuracy of the local-density approximation for the charge-transfer dynamics from these calculations.

The outline of this paper is as follows. In Sec. II, we present basic equations of the time-dependent mean-field theories, and a method to evaluate the charge-transfer probability. We also describe our numerical method to solve the equation, the real-space and real-time method in detail. In Sec. III, we give our calculated results. We first present the TDLDA calculations to show the electronic dynamics in the collision. We also discuss numerical aspects and the accu-

racy and convergence of our calculations. We then present results with an improved treatment of the exchange effect, and discuss the significance of the nonlocal nature of the exchange. Finally in Sec. IV, a summary is presented.

II. FORMULATION

A. Time-dependent mean-field equations

We describe the Ar^{8+}-Ar collision in the effective time-dependent single-particle picture. We treat eight valence electrons explicitly, assuming Ar^{8+} of the projectile ion and the target atom as an inert core. We employ the norm-conserving pseudopotential as an effective electron-ion interaction. The reason for using the pseudopotential is closely related to our numerical method to solve the time-dependent Schrödinger equation. To represent the single-electron wave function, we employ a three-dimensional uniform Cartesian mesh. The description of core orbitals in the mesh representation requires an extremely fine mesh, and cannot be accepted from the computational viewpoint. The use of the norm-conserving pseudopotential is a common technique in the electronic structure calculations of molecules and solids.

We assume the spin independence of the single-particle dynamics: two electrons occupy one spatial orbital throughout the collision. We thus treat four spatial orbitals. The time evolution is described by the following equation for the single-electron wave functions:

$$i\hbar\frac{\partial}{\partial t}\phi_i(\mathbf{r},t)=\left\{-\frac{\hbar^2}{2m}\nabla^2+v_P[\mathbf{r}-\mathbf{R}_P(t)]+v_T[\mathbf{r}-\mathbf{R}_T(t)]+e^2\int d\mathbf{r}'\frac{\rho(\mathbf{r}',t)}{|\mathbf{r}-\mathbf{r}'|}+\hat{W}\right\}\phi_i(\mathbf{r},t). \tag{1}$$

Here v_P and v_T represent the pseudopotential of the highly charged projectile ion and that of the core of the target, respectively. The density $\rho(\mathbf{r},t)$ is evaluated with the time-dependent wave function as

$$\rho(\mathbf{r},t)=2\sum_i|\phi_i(\mathbf{r},t)|^2. \tag{2}$$

$\hat{W}$ in Eq. (1) represents the effects of exchange and correlation. Its explicit form will be given in Sec. II B.

The theories we employ respect the Galilean invariance. We solve the equation in the frame where the projectile and target have velocities of the same magnitude and opposite directions, to save the computational resources—$\mathbf{R}_P(t)=\mathbf{V}t/2+\mathbf{b}/2$ and $\mathbf{R}_T(t)=-\mathbf{V}t/2-\mathbf{b}/2$—where $\mathbf{V}$ is the incident relative velocity between the projectile ion and target atom. $\mathbf{b}$ represents the impact parameter vector. A straight-line trajectory is assumed, and is appropriate for the incident energy region of our present interest.

We employ the norm-conserving pseudopotential produced with the procedure of Ref. [13] in a separable form [14] for v_P and v_T in Eq. (1). The separable potential has the following form:

$$v_{ps}(\mathbf{r},\mathbf{r}')=v_{loc}(r)\delta(\mathbf{r}-\mathbf{r}')+\sum_{lm}\frac{\Delta v_l^p(r)\phi_{lm}^p(\mathbf{r})\phi_{lm}^{p*}(\mathbf{r}')\Delta v_l^p(r')}{\int d\mathbf{r}|\phi_{lm}^p(\mathbf{r})|^2\Delta v_l^p(r)}. \tag{3}$$

The pseudopotential is constructed for each partial wave specified by the angular momentum l as $v_l^p(r)$. $\phi_{lm}^p(\mathbf{r})$ is the atomic wave function for the partial wave lm calculated with the pseudopotential. We calculate these up to $l=2$, and choose a certain component $v_l^p(r)$ as a local part $v_{loc}(r)$. $l=2$ will be used later. $\Delta v_l^p(r)$ is defined by $\Delta v_l^p(r)=v_l^p(r)-v_{loc}(r)$. Since the ion moves with a constant velocity, the atomic wave function $\phi_{lm}^p(\mathbf{r})$ needs to be boosted,

$$\phi_{lm}^p(\mathbf{r})=\exp\left[\frac{im\mathbf{V}_{ion}\cdot\mathbf{r}}{\hbar}\right]u_l^p(r)Y_{lm}(\hat{r}), \tag{4}$$

where $u_l^p(r)$ is a radial wave function of the atomic orbital. $\mathbf{V}_{ion}$ indicates the velocity of the ions, either $\mathbf{V}/2$ or $-\mathbf{V}/2$ for the projectile or target, respectively.

The initial condition is prepared by solving the static solution for the target Ar atom, putting projectile and target ions at certain initial positions. However, if we naively solve the static equation including both potentials by the projectile and target ions, the ground-state configuration would be such that both the projectile and target orbitals would be equally occupied by four electrons. To prepare the initial condition in which the target atom is occupied by eight electrons while the projectile has no electron, we solve the initial wave function within a spatial area excluding the region of the strong field of the projectile ion. We thus obtain the initial orbitals of target Ar atom which is distorted by the Coulomb field of the projectile ion. At the beginning of the time evolution, the initial wave function $\phi_i(t=T_{init})$ is given by the static solutions ϕ_i^{static} boosted with the velocity $-\mathbf{V}/2$:

$$\phi_i(t=T_{init})=\exp\left[\frac{-im\mathbf{V}\cdot\mathbf{r}}{2\hbar}\right]\phi_i^{static}. \tag{5}$$

B. Treatment of exchange and correlation

We will consider three kinds of time-dependent mean-field theories to describe the electronic dynamics of charge-transfer processes. The first is the TDHF theory, which is conceptually simple. We assume that the wave function of the system is given by a single Slater determinant throughout the collision. The time evolution of the single-electron wave functions is determined by the variational consideration. The Hamiltonian, however, includes a nonlocal Fock term whose computation requires much computational time. The $\hat{W}$ operator in Eq. (1) is given explicitly by

$$\hat{W}\phi_i(\mathbf{r},t)=-e^2\sum_j\left\{\int d\mathbf{r}'\frac{\phi_j^*(\mathbf{r}',t)\phi_i(\mathbf{r}',t)}{|\mathbf{r}-\mathbf{r}'|}\right\}\phi_j(\mathbf{r},t). \tag{6}$$

The second theory is the adiabatic time-dependent local-density approximation, which we abbreviate as the TDLDA. This is the easiest means from a computational point of view. $\hat{W}$ in Eq. (1) is a simple multiplication of the local potential,

$$\hat{W}\phi_i(\mathbf{r},t)=\mu_{xc}(\rho(\mathbf{r},t))\phi_i(\mathbf{r},t), \tag{7}$$

where μ_{xc} represents the same function of density as the static exchange-correlation potential. In practical calculations, we use the function proposed in Ref. [15].

The TDLDA has been applied successfully to excited states of various systems. However, there are several shortcomings in the simple local-density approximation. One is the incomplete cancelation of the self-interaction. This induces the self-consistent potential which damps exponentially instead of a proper Coulomb tail. Another difficulty is the electronic excitation around the threshold region. In the LDA, the orbital energy of the highest occupied state is much smaller than the ionization potential. Closely related to this fact, the excited states of molecules around the threshold region appears at too low an excitation energy [16]. Since the electron-transfer dynamics is sensitive to the orbital energy and the potential tail, we will examine in detail the influence of these shortcomings of the TDLDA on the charge-transfer processes.

In the TDHF calculation, the self-interaction is correctly canceled between the Hartree and Fock terms. As an approximate method to satisfy the self-interaction cancelleration in the local form, a prescription of self-interaction correction (SIC), has been widely used. For the time-dependent problem, the combined use of the SIC with the optimized effective potential (OPM) was proposed [11,12]. The OPM is approximately constructed with the procedure proposed by Krieger, Li, and Iafrate (KLI) [17]. The computational cost of this KLI-SIC approach is modest, a few times that of the TDLDA. In the KLI-SIC approach, the operation of $\hat{W}$ is the multiplication of a local potential constructed by the procedures [11,12]

$$\mu_{xc,\sigma}^{SIC}=\sum_i \frac{\rho_{i\sigma}(\mathbf{r},t)}{\rho_\sigma(\mathbf{r},t)}\{v_{i\sigma}(\mathbf{r},t)+[\overline{\mu}_{xc,i\sigma}^{SIC}(t)-\overline{v}_{i\sigma}]\}, \tag{8}$$

where $\rho_{i\sigma}$ is the density of ith orbital and spin σ. Other quantities are defined by

$$v_{i\sigma}(\mathbf{r},t)=\frac{\delta E_{xc}[\rho_\uparrow,\rho_\downarrow]}{\delta\rho_\sigma}-\int d\mathbf{r}'\frac{\rho_{i\sigma}(\mathbf{r}',t)}{|\mathbf{r}-\mathbf{r}'|}-\frac{\delta E_{xc}[\rho_{i\sigma},0]}{\delta\rho_{i\sigma}}, \tag{9}$$

$$\overline{\mu}_{xc,i\sigma}^{SIC}(t)=\langle\phi_{i\sigma}|\mu_{xc,\sigma}^{SIC}(\mathbf{r},t)|\phi_{i\sigma}\rangle, \tag{10}$$

$$\overline{v}_{i\sigma}(t)=\langle\phi_{i\sigma}|v_{i\sigma}(\mathbf{r},t)|\phi_{i\sigma}\rangle. \tag{11}$$

$E_{xc}[\rho_\uparrow,\rho_\downarrow]$ is the exchange-correlation energy density for spin-polarized electron gas. In the practical calculation, $[\overline{\mu}_{xc,i\sigma}^{SIC}(t)-\overline{v}_{i\sigma}]$ of Eq. (8) is calculated by solving the algebraic equation

$$\sum_{i=1}^{N_\sigma-1}(\delta_{ji,\sigma}-M_{ji,\sigma})(\overline{\mu}_{xc,i\sigma}^{SIC}-\overline{v}_{i\sigma})=\overline{V}_{j\sigma}-\overline{v}_{j\sigma},$$

$$j=1,\ldots,N_\sigma-1, \tag{12}$$

where N_σ is the number of orbitals for spin σ electrons, and

$$M_{ji,\sigma}=\int d\mathbf{r}\,\frac{\rho_{j\sigma}(\mathbf{r})\rho_{i\sigma}(\mathbf{r})}{\rho_\sigma(\mathbf{r})}, \tag{13}$$

$$\overline{V}_{i\sigma}=\left\langle\phi_{i\sigma}\left|\sum_{j=1}^{N_\sigma}\frac{\rho_{j\sigma}(\mathbf{r})v_{j\sigma}(\mathbf{r})}{\rho_\sigma(\mathbf{r})}\right|\phi_{i\sigma}\right\rangle. \tag{14}$$

C. Charge-transfer probability and cross sections

The description of the charge-transfer processes in the time-dependent mean-field equation is deterministic; we have one solution for a given impact parameter and incident energy. When the two ions are well separated after collision, the electron density distribution is usually well localized in the two spatial regions, around the projectile and the target ions, as we will see below. However, each single-electron wave function is not localized in one region but separated into spatial regions of the projectile and target ions. As a consequence, the Slater determinant wave function is not a product of two Slater determinants, one around the projectile ion and the other around the target ion, but is a superposition of such products. If one considers the Slater determinant wave function in a restricted spatial area, for example, inside a sphere of a certain radius around the target ion, it is not an eigenstate of any operators of the target ion, even of the number operator of electrons.

In a correct many-body description, the many-body wave function after collision should extend to many final channels specified by the internal states of the projectile and target ions. It may be natural to relate the components of the Slater determinant specified by the internal states of projectile and target ion to the respective channel components. However, we should note that there remains a spurious coupling among channels in the time-dependent mean-field description through the mean-field potential, which mixes electron densities of different channels, although there should be no interaction among different channels in a correct quantum-mechanical description of the asymptotic region. This is a well-known limitation of the one-body theories in describing the reaction.

Furthermore, since we are solving one-body dynamical equation, there is, in principle, no guarantee that the correlations obtained from the calculation beyond the one-body correlation can be physically reliable. In fact, in a description of the nucleus-nucleus collision in the TDHF theory, it is known that the measured variance of the transferred nucleons cannot be described adequately, though the measured mean value can be [18]. We should also note that, in contrast to the TDHF method, the Slater determinant wave function is only introduced as a reference state to represent the density in the density-functional theory, and is not considered as an approximation to the many-body wave function. Nevertheless,

we consider that procedure proposed in Ref. [19] is the most natural way to extract various reaction probabilities from the calculation.

We denote the Slater determinant wave function at the final stage of calculation as $\Psi(x_1, \ldots, x_N; b)$ for a specific incident energy E and impact parameter b. N is the number of electrons, $N=8$ in our case. x_i denotes spatial and spin coordinates of the ith electron. Let us consider the probability that n electrons out of total N are removed from the target atom. This is given by integrating the square of the Slater determinant with respect to coordinates of $N-n$ electrons over the spatial area T around the target ion and the coordinates of n electrons over the spatial area $\overline{T}$ which is outside the spatial area T:

$$P_n(b) = {}_N C_n \int_T d^4x_1 \cdots d^4x_n \times \int_{\overline{T}} d^4x_{n+1} \cdots d^4x_N |\Psi(x_1, \ldots, x_N; b)|^2. \tag{15}$$

As discussed in Ref. [19], the above probability can be calculated in terms of the single-electron matrix elements in the following way,

$$P_n(b) = \sum_{s(\overline{T}^n T^{N-n})} \begin{vmatrix} \langle \psi_1 | \psi_1 \rangle_{\tau s_1} & \cdots & \langle \psi_1 | \psi_N \rangle_{\tau s_1} \\ \vdots & \ddots & \vdots \\ \langle \psi_N | \psi_1 \rangle_{\tau s_N} & \cdots & \langle \psi_N | \psi_N \rangle_{\tau s_N} \end{vmatrix}. \tag{16}$$

Here τ_i represents either T or $\overline{T}$, and $\tau_1, \ldots, \tau_N$ specifies the sequence of the spatial area in calculating the matrix element. Summation over $s(\overline{T}^n T^{N-n})$ indicates that all the possible sequences of $\tau_1, \ldots, \tau_N$ should be considered on the condition that $\overline{T}$ appears n times and T appears $N-n$ times in the sequence. ψ_i represents the single-electron wave function including the spin part. The spatial part of the wave function ψ_i is denoted as ϕ_i, and is the solution of Eq. (1) at the final time of calculation. Equation (16) then reduces to

$$P_n(b) = \sum_{s(\tau_1 \cdots \tau_N : \overline{T}^n T^{N-n})} \begin{vmatrix} \langle \phi_1 | \phi_1 \rangle_{\tau s_1} & 0 & \cdots & \langle \phi_1 | \phi_M \rangle_{\tau s_1} & 0 \\ 0 & \langle \phi_1 | \phi_1 \rangle_{\tau s_2} & \cdots & 0 & \langle \phi_1 | \phi_M \rangle_{\tau s_2} \\ \vdots & \vdots & \ddots & \vdots & \vdots \\ \langle \phi_M | \phi_1 \rangle_{\tau s_{(N-1)}} & 0 & \cdots & \langle \phi_M | \phi_M \rangle_{\tau s_{(N-1)}} & 0 \\ 0 & \langle \phi_M | \phi_1 \rangle_{\tau s_N} & \cdots & 0 & \langle \phi_M | \phi_M \rangle_{\tau s_N} \end{vmatrix}, \tag{17}$$

where M is the number of spatial orbital, $M=N/2=4$ in our case.

The cross section that n electrons are removed from the target atom is calculated by integrating $P_n(b)$ over the impact parameter b;

$$\sigma_n = \int db\, 2\pi b P_n(b). \tag{18}$$

The total charge-transfer cross section is then obtained as

$$\sigma_{tot} = \sum_{n=1}^{N} \sigma_n. \tag{19}$$

The average number of removed electrons for the collision specified by the impact parameter b may be evaluated as

$$N_{av}(b) = \sum_{n=1}^{N} n P_n(b). \tag{20}$$

It is easy to prove that this value coincides with the loss of electrons from the target atom area which is calculated by integrating the electron density inside the spatial area T:

$$N_{av}(b) = N - \int_T d\mathbf{r} \rho(\mathbf{r}, T_{final}). \tag{21}$$

D. Numerical detail

We employ a finite-difference scheme both for space and time variables which was originally developed in nuclear theory more than 20 years ago [20]. For static electronic problems, the finite-difference method combined with the pseudopotential has been widely used [21]. One of the authors of the present paper extended the treatment to time-dependent electronic dynamics, discretizing the time variable as well [22]. The real space-time method offers an efficient scheme to calculate linear-response properties of finite [23] and infinite [24] systems, and to simulate collision dynamics [9].

For spatial coordinates, we discretize the three-dimensional Cartesian coordinates into a uniform mesh, and the grid points inside a large rectangular box are used to represent the single-electron wave functions. In this representation, the single-electron Hamiltonian is sparse. The local potential is represented by the diagonal matrix. There are two kinds of off-diagonal elements: the kinetic-energy operator and the nonlocal part of the pseudopotential. We employ

the higher-order finite-difference scheme, taking nine points for one direction to approximate the Laplacian operator. The treatment of the nonlocal pseudopotential was explained in detail in Ref. [21].

From a wave function at time t, $\phi_i(t)$, we construct the Hamiltonian $h(t)$. The short-time evolution of the wave functions is approximately achieved by this Hamiltonian. We further make a Taylor series expansion of the time evolution operator,

$$\phi_i(t+\Delta t) \approx \exp\left[-\frac{i}{\hbar}\Delta t\,\hat{h}(t)\right]\phi_i(t) \approx \sum_{k=0}^{N_{max}} \frac{1}{k!}\left(-\frac{i}{\hbar}\Delta t\,\hat{h}(t)\right)^k \phi_i(t), \qquad (22)$$

where we practically take $N_{max}=4$. The Taylor expansion up to a finite order violates the unitarity of the time evolution. However, we found that during the period of our calculation here, the orthonormalization of the single-electron wave function is kept to high accuracy during the time evolution without an explicit orthonormalization procedure. Since this method of time evolution is a type of explicit method, we need to use sufficiently small time steps Δt satisfying $\epsilon_{max}\Delta t \leqslant 1$, where ϵ_{max} is the maximum eigenvalue of the Hamiltonian. The largest eigenvalue is dominated by the kinetic-energy operator, and is scaled by the inverse square of the mesh size. With a mesh size of 0.25 Å, we found that $\Delta t/\hbar = 0.002$ eV^{-1} gives a stable time evolution. We take the xy plane as the reaction plane, and take the y direction as the incident direction. As an initial condition, we usually put two ions separated by 10 Å in the y direction and two separated by the distance of the impact parameter in the x direction. The time evolution is calculated until the two ions are separated again by 10 Å in the y direction.

At each time step, we need to construct the Hartree potential. Instead of integration over grid points, we calculate this by solving the Poisson equation

$$\nabla^2 V^H(\mathbf{r},t) = -4\pi e^2 \rho(\mathbf{r},t). \qquad (23)$$

We employ the conjugate gradient method to solve this equation. Since we are working in a finite box area, the iterative method requires a boundary value of the Hartree potential constructed by other method. For finite systems, the multipole expansion method is useful for this purpose. In the collision problem, the electron distribution is located around both projectile and target ions. Therefore, at each time step, we divide the whole spatial area into two areas, and make multipole expansion of the electron density around each ion.

The time evolution of the TDHF equation requires another technique. An explicit construction of the nonlocal Fock operator in the coordinate space representation is not appropriate because the number of grid points is very large. In Ref. [2], the exchange potential is treated by solving the Poisson equation without an explicit construction of the nonlocal Fock operator. A similar method was recently discussed to solve the static and time-dependent Hartree-Fock equations in a coordinate mesh representation [25]. The technique was also used to evaluate the exchange matrix elements [26,27]. The multiplication of the Fock operator to a wave function $\psi(\mathbf{r})$ may be expressed as

$$\int d\mathbf{r}'\, V^F(\mathbf{r},\mathbf{r}';t)\psi(\mathbf{r}') = \sum_j \phi_j(\mathbf{r},t)\chi_{ji}(\mathbf{r},t), \qquad (24)$$

where we define

$$\chi_{ji}(\mathbf{r},t) = \int d\mathbf{r}' \frac{e^2}{|\mathbf{r}-\mathbf{r}'|}\phi_j^*(\mathbf{r}',t)\psi(\mathbf{r}'). \qquad (25)$$

The functions $\chi_{ji}(\mathbf{r},t)$ satisfy the Poisson equation

$$\nabla^2 \chi_{ji}(\mathbf{r},t) = -4\pi e^2 \phi_j^*(\mathbf{r},t)\psi(\mathbf{r}). \qquad (26)$$

We solve this again by the conjugate gradient method. We can thus avoid an explicit construction of the Fock operator in calculating the time evolution of the wave function, although we need to solve the Poisson equation many times.

III. RESULTS AND DISCUSSIONS

A. TDLDA calculation

Since numerical calculation is the easiest in the TDLDA, we made extensive calculations with the TDLDA for various physical conditions, and examined the convergence of the calculation with respect to several computational parameters. In the short note of Ref. [3], we presented TDLDA results stressing a comparison with measurements.

To illustrate the electronic dynamics intuitively, we first show contour plots of the electron-density distribution during collision for various incident ion energies and impact parameters. In Fig. 1 we show the time evolution of the electron density in the reaction plane, the x-y plane, for three incident ion energies: 18.4, 400, and 3200 keV. These correspond to incident ion velocities in atomic units, of 0.14, 0.64, and 1.80 a.u, respectively. The impact parameter is fixed at 4 Å. The calculations are achieved by taking grid points inside a rectangular box of $24\times40\times12$ Å^3 for $x\times y\times z$, and a mesh spacing of 0.25 Å. Four plots are shown at distances of two ions in a longitudinal direction specified by $2y$. The electronic dynamics is seen to change considerably across an incident ion velocity of about 1 a.u. In the two cases of lower incident ion energies, 18.4 and 400 keV, almost all the electrons removed from the target atom transfer to the projectile ion, while very few electrons are emitted to the continuum. The electron density is almost axially symmetric at each time step in the 18.4-keV case. These features are consistent with the picture of a classical overbarrier model, in which the electron-transfer process is considered in a static picture. The axial symmetry is violated at a higher incident energy, reflecting the growing importance of the incident velocity effect. In the 3200-keV case, we find a large electron flux outgoing in the transverse direction. At the right box boundary in the bottom panel of the figure, a fictitious reflection of the electron flux is seen. The electron density during the collision also strongly violates the axial symmetry. Since the velocity of the incident ion is faster than the typical velocity

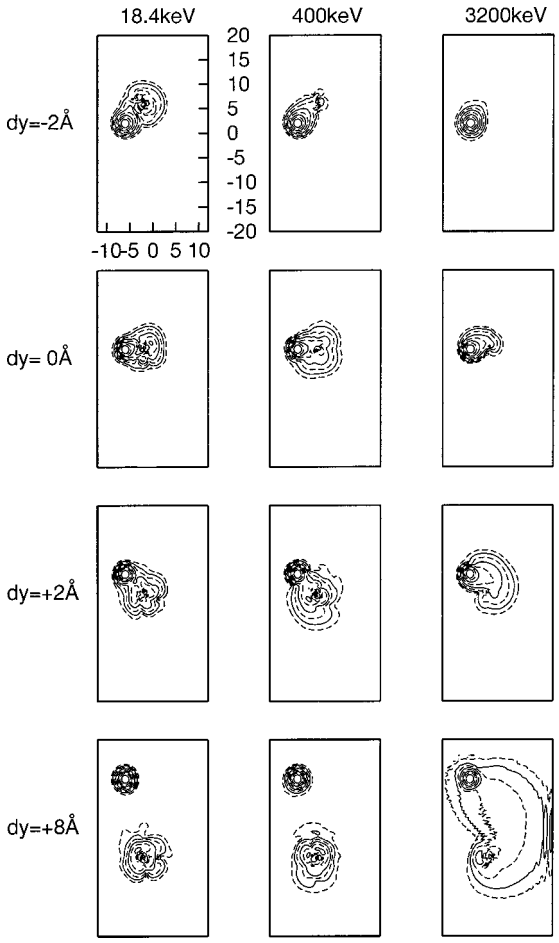

FIG. 1. The time evolution of the electron-density distribution of an Ar^{8+}-Ar collision for three incident energies at an impact parameter of 4 Å. The reaction proceeds from top to bottom. Four snapshots of the electron density in the reaction plane are shown at the distance of two ions in the longitudinal direction specified in the left. The electron contour plots are drawn at 1.0, 0.04, 0.0016, and 0.000 064 $Å^{-3}$ by solid curves, and at 0.2, 0.008, 0.00032, and 0.000 012 8 $Å^{-3}$ by dashed curves.

of valence electrons in the target in this case, the electrons cannot follow the Coulomb field of the projectile ion, and are emitted to the continuum.

In Fig. 2 we show the time evolution of the electron density for different impact parameter collisions, $b=2$, 4, and 6 Å, for a fixed incident ion energy of 400 keV. At the small impact parameter $b=2$ Å, both the target and projectile ions are seen to be highly excited after collision. We also see the electron distribution extending to the whole spatial area. Though the time length of our calculation is not long enough to see the final result of the collision, we may expect that some part of the electrons is emitted to the continuum even when the incident energy is rather low. For an impact parameter of 4 Å and outside, the target ion remains at a low excitation while the projectile ion has a spatially extended, highly excited structure. The formation of the highly excited state in the projectile ion after collision is again consistent with the picture in the classical overbarrier picture. That is, the electrons in the target atom transfer to the orbitals of the

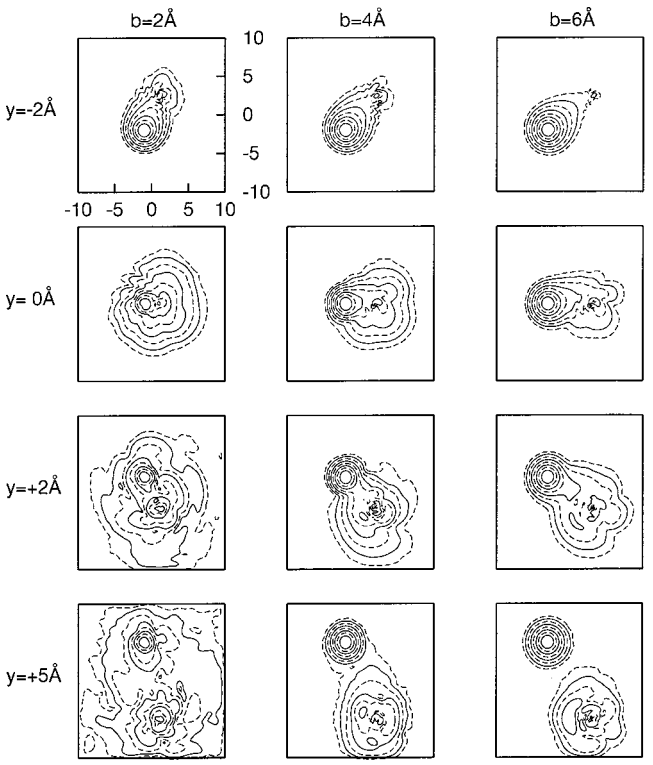

FIG. 2. The time evolution of the electron density of an Ar^{8+}-Ar collision for three impact parameters at an incident ion energy of 400 keV. Other features are the same as in Fig. 1.

projectile ion, which are approximately degenerate to the initial orbital of the target atom. For a highly charged ion, these orbitals correspond to highly excited ones.

The calculations given in Fig. 2 are achieved by employing a spatial area of $20\times20\times10$ $Å^3$ and a mesh size of 0.25 Å. The spatial area is smaller than that in Fig. 1. We found physical quantities, such as the number of electrons removed from the projectile ion, coincide well between two calculations. We thus see that the calculation of the present box size is large enough to obtain convergent results.

We next show, in Fig. 3, the average number of electrons around the projectile and target ions during the collision. We take a sphere of radius R around each ion, and integrate the electron density inside the sphere. We plot the calculated number of electrons around the projectile ion in Fig. 3(a), and that around the target ion in Fig. 3(b), as functions of the longitudinal distance between the projectile and target ions. The collision energy and impact parameter are fixed at 400 keV and 4 Å, respectively. This corresponds to the middle plots of Figs. 1 and 2. Four spheres of radii 3, 4, 5, and 6 Å are used to calculate the electron number. From Fig. 3(b), we see that all the electrons are inside a sphere of 3 Å if the longitudinal distance of two ions y is greater than 4 Å. Reflecting the spatially extended density distribution of the projectile ion after collision, a sphere of more than 4-Å radius gives a convergent number of electrons around the projectile, as seen in Fig. 3(a). We see that the number of electrons transferred to the projectile ion is to a high accuracy independent of time after two ions are separated in a longitudinal direction greater than 4 Å. This indicates that elec-

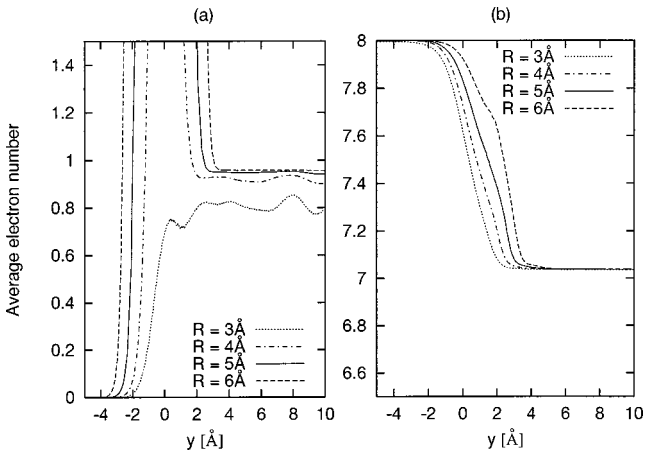

FIG. 3. The number of electrons inside a sphere of radius R around the projectile ion (a) and around the target ion (b) as a function of the longitudinal distance between the projectile and target ions. The incident energy and impact parameter are set to 400 keV and 4Å, respectively.

trons are not emitted to the continuum after two ions are well separated, at least within the time period of the present calculation. Therefore, although the calculated projectile ion shows a spatially extended, highly excited electronic structure, no Auger emission of electrons is described in the present TDLDA calculation. This may be expected, since the TDLDA is a kind of mean-field theory which does not allow any change of the occupation of the orbitals. To describe Auger emission processes, a treatment beyond the mean-field theory would be necessary, on which introduces an electron-electron collision term, for example.

In Fig. 4 we show the number of electrons around the projectile and target ions as a function of the impact parameter for the incident ion energy of a 400-keV collision. We take spheres of radius 5 Å around two ions, which is large enough to obtain convergent results, as we saw in Fig. 3. We

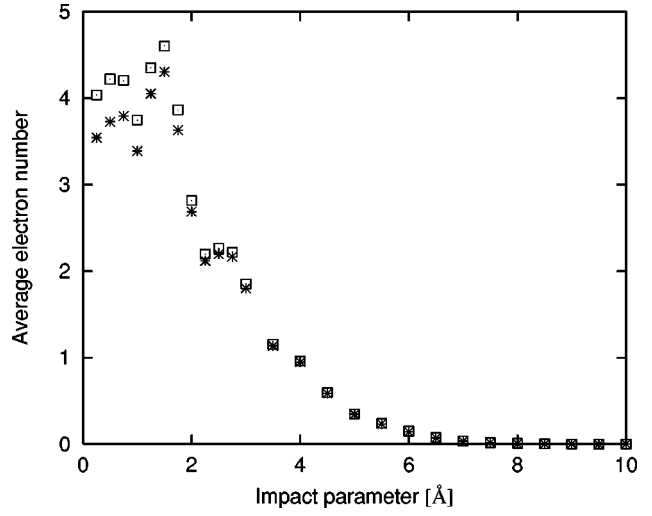

FIG. 4. The number of electrons removed from the target atom is shown by boxes, and the number of electrons transferred to the incident ion is shown by asterisks, as a function of the impact parameter. The incident ion energy is set to 400 keV.

show the number of electrons gained by the projectile ion with asterisks, and the number of electrons lost by the target ion with boxes. Inside an impact parameter of 2 Å, both the numbers of electrons around the projectile and the target ions are approximately equal to four, half the number of valence target electrons. This is again consistent with the picture of the classical overbarrier model. In this model, the formation of a moleculelike configuration is assumed during the collision. For small impact parameter collisions, all the valence electrons take part in the formation of a molecularlike state, and the information about the incident channel is lost at that stage. The electrons are then separated equally into a projectile and a target. We also note that the numbers of removed electrons and transferred electrons are very close, confirming that a very small fraction of electrons is emitted to the continuum for all impact parameter regions.

We finally discuss the numerical checks we achieved for some numerical and physical parameters to see the reliability of our results. As discussed in Figs. 1 and 2, we compared results between different box sizes to confirm that the artificial box boundary does not play a role. We also calculated with different mesh sizes. Calculations with mesh sizes of $h=0.3$ and 0.25 Å were found to give basically the same result for the charge-transfer probabilities and cross sections, though details of the time evolution of the electron density may differ slightly, especially around spatial regions close to the ion. We also achieved calculations with different time steps. As we noted, the time step should be smaller than the inverse of the maximum eigenvalue of the Hamiltonian for a stable iteration. As long as we used a time step small enough for stable iteration, we found that the results depend little on the choice of the time step.

We next discuss the construction of the electron-ion interaction. Although the construction of the norm-conserving pseudopotential is a well-established issue in condensed-matter theory, we employ it in rather different situation. That is, two ions move toward each other with velocities of around 1 a.u. Furthermore, two ions may come close to each other during the collisions, even inside the radius of the core electrons. How the core electrons affect the electronic dynamics in such situations is beyond our present approach. We simply anticipate that, since the radius of the core electrons is not very large, about 1 Å, only a limited cross section is influenced by the core electron dynamics, at most $\pi(2R_{core})^2 \sim 12$ Å^2.

We usually employ a psuedopotential constructed with a radius of connection at 1.05Å. To see the sensitivity of our results on the choice of this radius, we calculated the cross section of the charge transfer with a pseudopotential of larger connection radius, 1.61 Å. A comparison between different choices of pseudopotential is summerized in Table I. We see that the difference is very small.

In the construction of a separable pseudopotential in Eq. (3), we choose one of the partial-wave potentials to be used as a local part. We usually use the largest angular momentum component $l=2$. We made calculations with other angular momentum components as a local part, and compared results in Table I. The difference is again very small. Therefore, the calculation depends little on the construction of the electron-

TABLE I. The dependence of results on the construction of the pseudopotential. The cross sections of total as well as one to eight electron removal from the target atom are compared. Three different angular momentum components of $l=0, 1$, and 2 are used as local potentials in the three left columns with a pseudopotential constructed with radius 1.05 Å. The last column is with the pseudopotential of larger radius of 1.61 Å. The incident Ar^{8+} energy is set to 400 keV, and the impact parameter to 4 Å.

	Rps 1.05 Å ($l=0$)	Rps 1.05 Å ($l=1$)	Rps 1.05 Å ($l=2$)	Rps 1.61 Å ($l=2$)
1	34.30	33.84	34.18	33.69
2	16.13	16.18	16.18	15.69
3	8.94	9.33	9.00	9.27
4	5.28	5.60	5.43	6.30
5	3.00	3.15	3.18	3.70
6	1.38	1.40	1.44	1.54
7	0.40	0.39	0.39	0.39
8	0.05	0.05	0.05	0.04
Total	69.48	69.94	69.84	70.76

ion potential, so long as the core electrons do not play an important role.

B. Improved treatments of the exchange potential

In this section, we discuss calculations with improved treatments of the exchange effect. We will consider, beyond the TDLDA, the self-interaction correction method in the time-dependent optimized effective potential approach (KLI-SIC approach), and a full calculation of the nonlocal exchange potential in the TDHF approach. Since the TDHF calculation requires much more computational time than the TDLDA calculation, the results shown below are calculated with a smaller box size and coarser mesh spacing. The box area is $14\text{Å}\times 14\text{Å}\times 7\text{Å}$, and the mesh spacing is 0.3Å. Even at this box size, the charge-transfer probabilities do not differ much from calculations with a larger box size. As we noted, the results also do not change much from those found at smaller mesh sizes, though the details of the dynamics, such as the electron-density distribution around the ion, may change slightly.

We first show the orbital energies of the isolated atom in Table II. The LDA calculation gives a $3p$ orbital energy of 10.33 eV, much smaller than the ionization potential of the Ar atom: 15.76 eV. In the Hartree-Fock calculation, the $3p$ orbital energy is 16.10 eV, close to the experimental ionization potential. We made calculations of the optimized effective potential in the KLI procedure with the self-interaction correction Hamiltonian. We achieved two calculations, with and without the correlation effect as a local potential, and show these in the table. The KLI-SIC calculation gives a $3p$ orbital energy close to the ionization potential, and is regarded as a good approximation of the Hartree-Fock calculation.

TABLE II. Orbital energies of static calculations by the Hartree-Fock (HF) method, the self-interaction correction method with exchange-only (KLI-SIC, X), and exchange and correlation (KLI-SIC, XC), and the local-density approximation (LDA) are compared.

	HF	KLI-SIC (X)	KLI-SIC (XC)	LDA
$3s$	34.93	28.61	29.41	24.18
$3p$	16.10	14.70	15.49	10.33

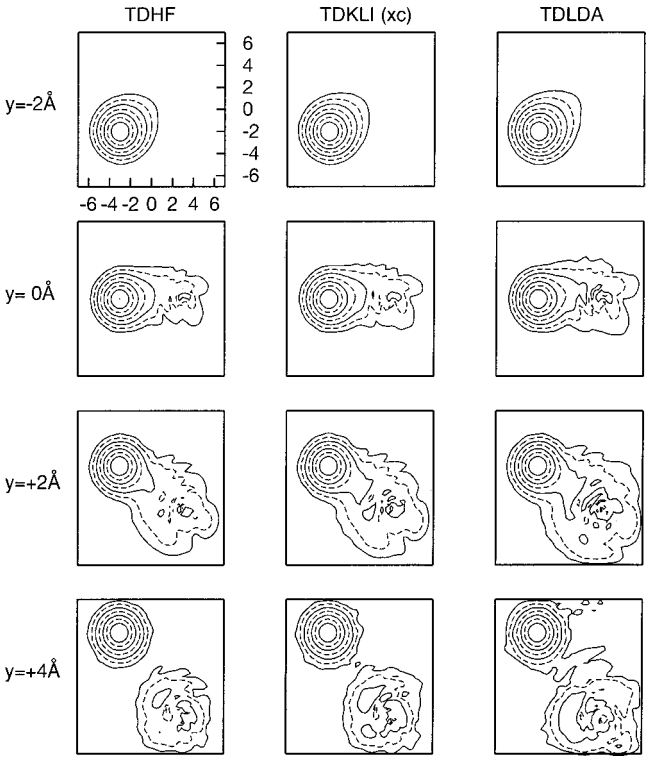

FIG. 5. The time evolution of the electron density of an Ar^{8+}-Ar collision by three different treatments of exchange. The incident ion energy is set to 400 keV, and the impact parameter is 6 Å. Other features are the same as those in Fig. 1 except that the lowest contour line is not drawn.

In Fig. 5 we show the time evolution of the electron-density distribution calculated with the three methods. The incident ion energy is set at 400 keV, and the impact parameter is 6Å. The three calculations used the TDHF, and KLI-SIC methods, in which the correlation effect is included as a local potential, and the TDLDA. Basically they give very similar results to each other. Looking into details, the spatial extension of the electron distribution around the projectile ion is more extended in the TDLDA calculation than the others. This may be understood as originating from the smaller orbital energy in the static LDA calculation. In the classical overbarrier picture, the electrons are expected to transfer to the orbitals of projectile ion, which are approximately degenerate to the initial target orbital. Therefore, the smaller binding in the LDA calculation gives a transfer to the orbitals of smaller binding in the projectile ion, which in turn gives a spatially extended density distribution.

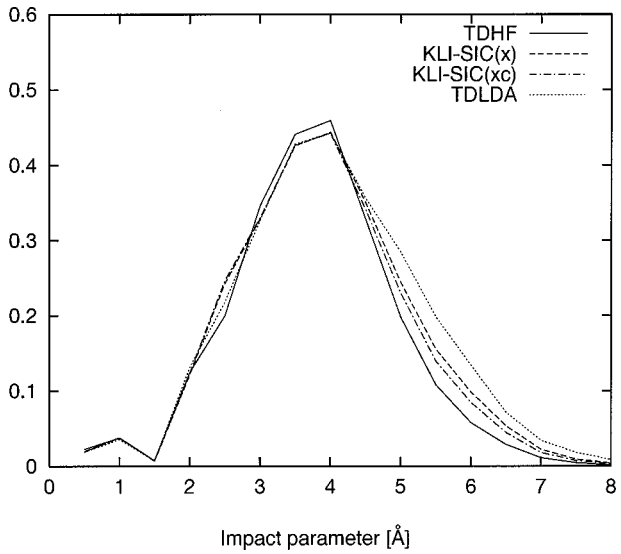

FIG. 6. One-electron removal probability from the target atom as a function of the impact parameter. Calculations with different treatments of exchange are compared. The incident ion energy is set to 400 keV.

We next show, in Fig. 6, the probability of one-electron removal from the target atom as a function of the impact parameter for a fixed energy collision at 400 keV. The large difference is seen in collision at a large impact parameter. The TDLDA calculation gives the largest probability, and the TDHF calculation gives the smallest. The KLI-SIC calculation with and without local correlation potential lies between the two. The accurate treatment of the nonlocal exchange potential thus has a large effect on the one-electron transfer probability at a large impact parameter. In contrast, the correlation effect treated as a local potential plays a minor role for this quantity, as we learn from the small differences between the KLI-SIC calculations with and without the correlation effect. For electron-transfer probabilities of two and more electrons, the difference is found to be much smaller among the different treatments of exchange.

We see the order of the electron-transfer probability, the largest TDLDA and the smallest TDHF, is the same as that of the static orbital energies shown in Table II. There are two aspects of the treatment of the exchange that may be expected to affect the charge-transfer probability. One is the change of the orbital energy. Since the orbital energy becomes lower in the correct treatment of the exchange, the reduction of the charge-transfer probability is expected. The other aspect is the correct behavior of the potential tail. The correct treatment of the exchange gives a potential with the correct $1/r$ behavior. The increase of the attractive potential is expected to reduce the potential barrier and to increase the charge-transfer probability. Our numerical results indicate that the former effect, the reduction of the charge-transfer probability due to the increase of the orbital binding energy, is more crucial for the charge-transfer probability.

The KLI-SIC approach is known as a good approximation of the static orbital calculation [17], and indeed reproduces rather well the orbital energy by the Hartree-Fock calculation, as shown in Table II. However, we find that the charge-transfer probability from the KLI-SIC calculation is not very close to the TDHF calculation, but lies around the middle between the TDHF and TDLDA calculations. Therefore, we conclude that the KLI-SIC method is not a very good approximation to the TDHF for the charge-transfer probability, though it works to improve the TDLDA result to some extent.

TABLE III. The cross sections of electron removal from the target atom are calculated with different treatments of the exchange.

No. of electrons	TDHF	KLI-SIC (X only)	KLI-SIC (XC)	TDLDA
1	28.09	31.42	30.24	34.36
2	14.78	14.80	14.43	15.83
3	7.88	8.07	7.95	8.53
4	4.67	4.85	4.80	4.98
5	2.78	2.95	2.93	2.96
6	1.34	1.49	1.48	1.47
7	0.41	0.48	0.48	0.47
8	0.06	0.07	0.07	0.07
Total	60.00	64.13	62.39	68.68

In Table III we show the cross sections of electron removal from the target atom calculated by different theories. The incident energy is fixed at 400 keV. As noted above, the difference is the largest for the one-electron removal, and it amounts to about 20% between the cross sections of TDHF and TDLDA methods. The difference is much smaller for the multiple charge removal. The difference of the total charge transfer thus reflects mainly that of the one-electron removal, and is about 10–15 %.

For the multiple electron-transfer process, the second and higher ionization potentials are relevant in the classical overbarrier model. In the static calculations, the difference of the first and second ionization potentials reflects mainly the Hartree potential of the highest occupied orbital. Therefore, the difference between the orbital energy and the ionization potential in the LDA calculation becomes less significant for the second ionization potential and higher. This fact is considered to explain the small difference of the electron removal cross sections of two and more electrons.

For singly and doubly charged ions, a much larger difference in the cross sections was reported depending on the treatment of exchange effect [10]. We expect that this large difference originates from the discrete nature of the orbitals of singly and doubly charged projectile ions. That is, for singly and doubly charged ions, the density of levels in the projectile ion is not high; the final states to be occupied by the transferred electrons are rather limited. In this case, the charge-transfer probability is considered to depend crucially on the difference of the orbital energies in the projectile and target. Since the different treatment of exchange causes large changes of the orbital energies, it may have a large effect on the charge-transfer probability depending on whether or not there are orbitals of the projectile ion which are approximately degenerate to the orbitals of the target atom. Con-

versely, in our present study of the electron transfer to a highly charged ion, the density of states in the highly charged projectile ion is very high and the effects related to the discrete nature of the projectile ion orbitals are expected to be small. We thus consider that our conclusion, that different treatments of the exchange effect produce the differences in the one-electron removal cross section by 20% does not contradict Ref. [10], which reported a much larger effect for singly and doubly ionized projectiles.

IV. SUMMARY

We have presented time-dependent mean-field calculations of charge-transfer reactions between a highly charged ion and atom, taking Ar^{8+} and Ar as examples. A direct method is employed to solve the time-dependent mean-field equation in real-space and real-time. We employ the same Hamiltonian as that in first-principles calculations of the electronic ground states of condensed-matter systems. The calculation includes no empirical parameter, and we can microscopically describe the electronic dynamics of the multiple electron-transfer processes. The time evolution of the electron-density distribution also provides us with an intuitive picture of the dynamics.

We have elucidated basic dynamics of the charge-transfer processes by showing results for various incident ion energies and various impact parameters in the adiabatic time-dependent local-density approximation. For reactions of incident ion velocities below 1 a.u. and not very small impact parameters, the reaction dynamics is consistent with the picture of classical overbarrier model. At higher incident energies, the change of the dynamics is observed from the transfer to the continuum emission. To see the significance of the correct treatment of the exchange effect, two methods with improved treatments of the exchange effect have been considered beyond the simple adiabatic local-density approximation: a self-interaction correction approach and a full nonlocal treatment of exchange in the time-dependent Hartree-Fock theory. The correct nonlocal treatment of exchange has the largest effect on the one-electron transfer probability and is found to reduce the one-electron removal cross section by about 20% compared to the calculation by the adiabatic time-dependent local-density approximation.

ACKNOWLEDGMENTS

This work was supported by the Ministry of Education, Science, and Culture, Japan, Contract No. 11640372. We acknowledge the Institute of Solid State Physics, University of Tokyo, and the Research Center for Nuclear Physics, Osaka University, for the use of supercomputers.

[1] A. Niehaus, J. Phys. B **19**, 2925 (1986).
[2] W. Stich, H.J. Lüdde, and R.M. Dreizler, J. Phys. B **18**, 1195 (1985).
[3] R. Nagano, K. Yabana, T. Tazawa, and Y. Abe, J. Phys. B **32**, L65 (1999).
[4] E. Runge and E.K.U. Gross, Phys. Rev. Lett. **52**, 997 (1984).
[5] A. Zangwill and P. Soven, Phys. Rev. A **21**, 1561 (1980).
[6] W. Ekardt, Phys. Rev. Lett. **52**, 1925 (1984).
[7] Z.H. Levine and A.C. Allan, Phys. Rev. B **43**, 4187 (1991).
[8] C.A. Ullrich, P.-G. Reinhard, and E. Suraud, J. Phys. B **31**, 1871 (1998).
[9] K. Yabana, T. Tazawa, P. Bozek, and Y. Abe, Phys. Rev. A **57**, R3165 (1998).
[10] T. Kirchner, L. Gulyas, H.J. Lüdde, E. Engel, and R.M. Dreizler, Phys. Rev. A **58**, 2063 (1998).
[11] C.A. Ullrich, U.J. Gossmann, and E.K.U. Gross, Phys. Rev. Lett. **74**, 872 (1995).
[12] X.-M. Tong and S.-I. Chu, Phys. Rev. A **55**, 3406 (1997).
[13] N. Troullier and J.L. Martins, Phys. Rev. B **43**, 1993 (1991).
[14] L. Kleinman and D. Bylander, Phys. Rev. Lett. **48**, 1425 (1982).
[15] J. Perdew and A. Zunger, Phys. Rev. B **23**, 5048 (1981).
[16] M.E. Casida, C. Jamorski, K.C. Casida, and D.R. Salahub, J. Chem. Phys. **108**, 4439 (1998).
[17] J.B. Krieger, Y. Li, and G.J. Iafrate, Phys. Rev. A **45**, 101 (1992).
[18] J.W. Negele, Rev. Mod. Phys. **54**, 947 (1982).
[19] H.J. Lüdde and R.M. Dreizler, J. Phys. B **16**, 3973 (1983).
[20] H. Flocard, S. Koonin, and M. Weiss, Phys. Rev. C **17**, 1682 (1978).
[21] J.R. Chelikowsky, N. Troullier, and Y. Saad, Phys. Rev. Lett. **72**, 1240 (1994).
[22] K. Yabana and G.F. Bertsch, Phys. Rev. B **54**, 4484 (1996).
[23] K. Yabana and G.F. Bertsch, Int. J. Quantum Chem. **75**, 55 (1999).
[24] G.F. Bertsch, J.-I. Iwata, A. Rubio, and K. Yabana, Los Alamos e-print cond-mat/0005512.
[25] T. Matsuse, in *Proceedings of the International Symposium on Innovative Computational Methods in Nuclear Many-Body Problems* (World Scientific, Singapore, 1998), p. 369.
[26] I. Vasiliev, S. Ogut, and J.R. Chelikowsky, Phys. Rev. Lett. **82**, 1919 (1999).
[27] S. Takami, K. Yabana, and K. Ikeda, Prog. Theor. Phys. **94**, 1011 (1995).